

GO-N3RDet: Geometry Optimized NeRF-enhanced 3D Object Detector

Zechuan Li^{1,2}, Hongshan Yu^{1*}, Yihao Ding², Jinhao Qiao¹, Basim Azam², Naveed Akhtar²

¹Hunan University, ²The University of Melbourne

{lizechuan, yuhongshan, qiaojh}@hnu.edu.cn

{yihao.ding.1, basim.azam, naveed.akhtar1}@unimelb.edu.au

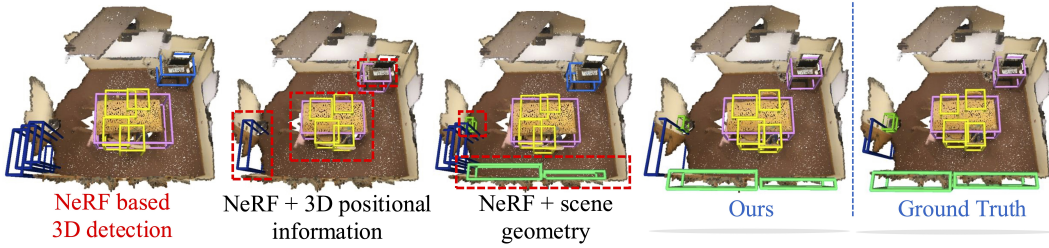


Figure 1. The paradigm of exploiting Neural Radiance Fields (NeRF) for multi-view 3D object detection suffers from critical issues of lack of 3D positional information modeling and insufficiency of scene geometry perception, leading to under par performance by methods like NeRF-Det [42] (left-most). We show that resolving these issues exclusively improves 3D object detection (dotted red boxes).

Abstract

We propose *GO-N3RDet*, a scene-geometry optimized multi-view 3D object detector enhanced by neural radiance fields. The key to accurate 3D object detection is in effective voxel representation. However, due to occlusion and lack of 3D information, constructing 3D features from multi-view 2D images is challenging. Addressing that, we introduce a unique 3D positional information embedded voxel optimization mechanism to fuse multi-view features. To prioritize neural field reconstruction in object regions, we also devise a double importance sampling scheme for the NeRF branch of our detector. We additionally propose an opacity optimization module for precise voxel opacity prediction by enforcing multi-view consistency constraints. Moreover, to further improve voxel density consistency across multiple perspectives, we incorporate ray distance as a weighting factor to minimize cumulative ray errors. Our unique modules synergetically form an end-to-end neural model that establishes new state-of-the-art in NeRF-based multi-view 3D detection, verified with extensive experiments on ScanNet and ARKITScenes. Code will be available at <https://github.com/ZechuanLi/GO-N3RDet>.

1. Introduction

Multi-view 3D object detection [11, 34, 42] uses multiple camera perspectives to enable a detailed understanding of

complex indoor environments, providing richer information than monocular [14, 22, 46] or 2D detection [9, 17, 29, 51]. Employing low-cost cameras instead of costly LiDAR or depth sensors [16, 24, 25, 50] makes this paradigm of 3D object detection practically appealing. Hence, it's a preferred choice in indoor robot navigation [35], scene understanding [23, 49] and augmented reality [19, 21].

A critical sub-task in multi-view 3D object detection is constructing 3D feature volumes from multi-view images. To that end, the pioneering approach of ImVoxelNet [31] first generates a voxel grid and projects the voxel centers onto multi-view images to extract features, which are then interpolated and aggregated using average pooling across views. ImGeoNet [34] builds further on this concept by incorporating supervisory signals to refine geometric perception from multi-view images, mitigating the ambiguity caused by free-space voxels.

More recently, methods exploiting Neural Radiance Fields (NeRF) [20] have demonstrated significant potential to capture the geometric structure of scenes for 3D object detection [12, 13, 42]. For instance, NeRF-Det [42] predicts scene opacity through NeRF, which allows dynamic adjustment of voxel features. By integrating the detection and NeRF branches via a shared MLP, NeRF-Det provides more accurate opacity predictions for the voxels. NeRF-Det++ [12] and NeRF-DetS [13] later enhanced the NeRF processing branch to further improve 3D scene understanding. Nevertheless, the NeRF-based stream of methods lacks

* Corresponding author: Hongshan Yu.

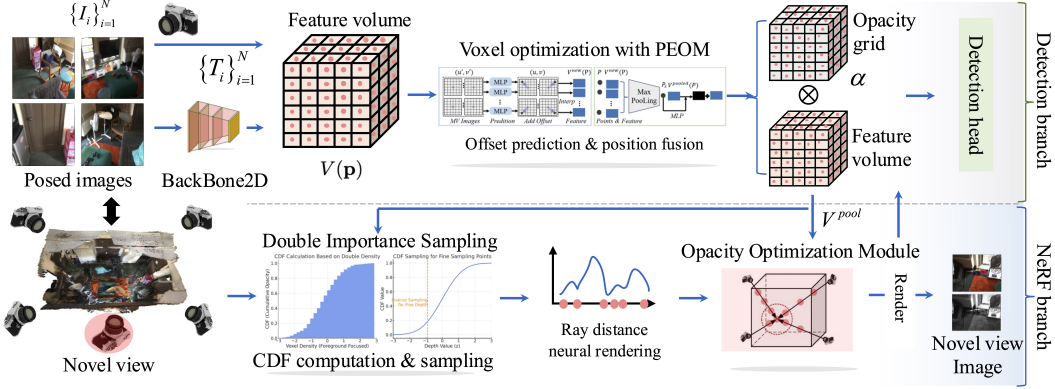


Figure 2. **Schematics of GO-N3RDet:** Given N input multi-view images $\{I_i\}_{i=1}^N$, we first project them onto a regular 3D grid, assigning each voxel N corresponding image features. The proposed Positional information Embedded voxel Optimization Module (PEOM) fuses these features and optimizes the voxel positions. In the NeRF branch, Double Important Sampling (DIS) is employed to focus on more foreground points, and opacity is optimized using the Opacity Optimization Module (OOM). The optimized opacity is used to adjust the fused voxel features, which are finally fed into the detection head.

in two major aspects, mentioned below.

(1) *Deficiency of 3D positional information:* 2D image features lack the necessary spatial information for precise 3D object localization. (2) *Insufficient scene geometry perception:* NeRF [20] focuses on scene-level rendering, neglecting object-level details crucial for object detection. This results in imprecise opacity predictions, which leads to poor 3D object detection. Both problems exclusively impact the detection performance - see Fig. 1. We also verify this in our experiments § 4 (Tab. 4), affirming inadequate opacity estimation for the detection task.

Addressing the challenges, we propose a Geometry Optimized NeRF-enhanced 3D Object Detector (GO-N3RDet) - see Fig. 2. Our technique is an end-to-end multi-view 3D object detection network that comprises multiple proposed constituent modules. It features a Positional information Embedded voxel Optimization Module (PEOM) to effectively construct voxels for 3D detection, enabling finer geometric details in voxel representation. We also propose a Double Importance Sampling (DIS) module, which considers two density components during sampling: the density at the adjusted voxel center and the density estimated by NeRF. This enhances opacity predictions by focusing on key foreground points while ensuring broad scene coverage. Moreover, we also introduce an Opacity Optimization Module (OOM) to enforce consistency across multiple views by minimizing the variance in opacity predictions for the same location viewed from different angles, promoting smoother scene reconstruction. In GO-N3RDet, voxel opacity is further refined by weighting multi-view opacity predictions based on ray length, reducing cumulative error and enhancing the precision of our 3D object detector.

We establish the effectiveness of our method by evaluating it on ScanNet [7] and ARKitScenes [1] datasets. Highlights of our contributions include the following.

- We propose GO-N3RDet - an end-to-end trainable network for multi-view 3D object detection. Our model uniquely leverages positional information embedded voxels and a geometrically optimized NeRF branch.
- We propose PEOM module to effectively embed scene positional information in 3D feature volumes, and introduce a DIS module for geometrically meaningful sampling for NeRF. Moreover, we introduce OOM module to ensure cross-perspective opacity consistency for opacity grid optimization.
- We establish new state-of-the-art (SOTA) in NeRF-based multi-view 3D detection on ScanNet and ARKitScenes, also showcasing a considerable training compute advantage over the best performing ray-matching method [33] while retaining performance.

2. Related Work

Point Cloud Based Object Detection. Due to the more reliable geometric information provided by 3D point clouds, point cloud-based methods [27,28,45] have demonstrated promising performance in indoor 3D object detection. These methods primarily follow two pipelines: *point-based methods* and *grid-based methods*. In the point-based methods, most approaches follow the pipeline introduced by VoteNet [26], which involves first voting for the object centers and then predicting the 3D bounding boxes and object categories. Several subsequent methods, such as ML-CVNet [40] and others [5, 16, 39, 48], are improvements largely building on the VoteNet pipeline. Grid-based methods project discrete and unordered 3D points onto regular voxel representations, addressing the challenges posed by the sparse and irregular nature of point clouds. For instance, GSDN [8] employs sparse convolution to enhance the efficiency of 3D convolutions, with an encoder-decoder structure built from sparse 3D convolution blocks. FCAF3D [30]

builds on the basic architecture of GSDN [8], improving it with an anchor-free approach that claims to enhance both efficiency and performance. TR3D [32] designs an efficient sparse convolutional architecture, simultaneously leveraging point cloud and image features. While point cloud-based methods achieve strong performance, their reliance on high-cost 3D sensors significantly restricts their broader applicability.

Monocular Object Detection. The field of monocular object detection has received considerable attention due to its practicality and cost-effectiveness. Numerous monocular 3D object detection methods have been developed for outdoor autonomous driving applications [3, 4, 18, 36–38]. In indoor scenarios, PointFusion [43] enhances detection accuracy by integrating depth estimation and semantic segmentation into the detection process. COH3D [15] and Total3D [43] leverage three collaborative losses to jointly train 3D bounding boxes, 2D projections, and physical constraints, enabling real-time estimation of object bounding boxes, room layouts, and camera poses from a single RGB image. Implicit3D [47] addresses the common inaccuracies in shape and layout estimation encountered in complex and heavily occluded scenes by utilizing implicit networks. Monocular methods show promise but face challenges in accurately deriving depth and scale from a single viewpoint and are limited in handling occlusions.

Multi-view Object Detection. ImVoxelNet [31] was one of the first methods to construct voxel features from multiple views and apply 3D convolutional networks for object detection. However, its performance was limited by insufficient scene geometric information. Subsequent methods addressed this limitation. ImGeoNet [34] improved scene geometry estimation by supervising voxel weights, while PARQ [41] combined pixel-aligned appearance features with geometric information for iterative prediction refinement. NeRF-based methods, such as NeRF-RPN [11], use neural radiance fields to predict voxel opacity but suffer from complexity and underutilized multi-view advantages. NeRF-Det [42] merges the NeRF branch with the detection branch for end-to-end opacity prediction, improving voxel geometry. Yet, the absence of 3D information in multi-view image features leads to inaccurate opacity predictions. Later refinements [12, 13] enhance NeRF-Det but do not directly address the fundamental problems of this type of approach.

The recent CN-RMA [33] method captures scene geometry using Ray Marching Aggregation to improve 3D detection. However, it relies heavily on pre-trained 3D reconstruction and ground truth truncated sign distance function for supervision, hindering end-to-end training and requiring significantly longer training times compared to NeRF-based approaches. MVSDet [44] improves detection performance through plane-sweeping and soft-weighting mecha-

nisms. However, its use of fixed depth planes in detection limits its flexibility in handling varying viewpoints, thereby weakening its implicit geometry modeling capability compared to NeRF-based methods.

3. Proposed Approach

Problem Formulation: We follow [31, 42] in formalizing the problem. Let us denote the set of N images captured from different viewpoints by $\{I_i\}_{i=1}^N$. Corresponding camera parameters for each image are denoted by $\{T_i\}_{i=1}^N$, where T_i includes intrinsic and extrinsic parameters of the i -th camera. The objective is to estimate a set of 3D bounding boxes $\{B_j\}_{j=1}^M$ for M objects in the scene, where each bounding box B_j is defined by its center coordinates (x_j, y_j, z_j) , dimensions (w_j, h_j, l_j) , and orientation θ_j .

For this problem, we particularly aim to overcome the limitations of the prior art in accurate perception of the scene geometry. Our GO-N3RDet approach is designed to enhance voxel quality within a scene by leveraging NeRF along with a range of proposed constituent modules for precise 3D detection. An overview of our approach is provided in Fig. 2, and details are given below.

3.1. Feature volume construction

Our technique begins by extracting image features from each camera view using pre-trained 2D backbone network - ResNet [10]. We express this operation as

$$F_{I_i} = \text{BackBone2D}(I_i), \quad (1)$$

where $F_{I_i} \in \mathbb{R}^{h \times w \times C}$ is the C -channel 2D feature map for the i -th image. Next, we construct a voxel grid of size $N_x \times N_y \times N_z$, where each voxel center is located at coordinate $\mathbf{p} = (x, y, z)^\top$. We then project these voxel center coordinates onto the image feature maps of each view using the camera parameters T_i , resulting in projection locations denoted as (u, v) . This projection is performed as

$$(u, v) = \pi(T_i \mathbf{p}_h) = \left(\frac{(T_i \mathbf{p}_h)_x}{(T_i \mathbf{p}_h)_z}, \frac{(T_i \mathbf{p}_h)_y}{(T_i \mathbf{p}_h)_z} \right), \quad (2)$$

where $\mathbf{p}_h = [x, y, z, 1]^\top$ is the homogeneous coordinate of the voxel center, T_i is the projection matrix combining both intrinsic and extrinsic parameters of the i -th camera, and $\pi(\cdot)$ denotes the function that performs homogeneous normalization to obtain the pixel coordinates (u, v) . Once the voxel centers are projected onto the image feature maps, we perform feature interpolation at the corresponding pixel locations to obtain the voxel features as

$$V(\mathbf{p}) = \text{Interpolate}(F_{I_i}, (u, v)) \in \mathbb{R}^C, \quad (3)$$

where $V(\mathbf{p})$ represents the voxel feature at position \mathbf{p} , obtained by projecting onto the image feature map and applying interpolation. Given that there are N views and the

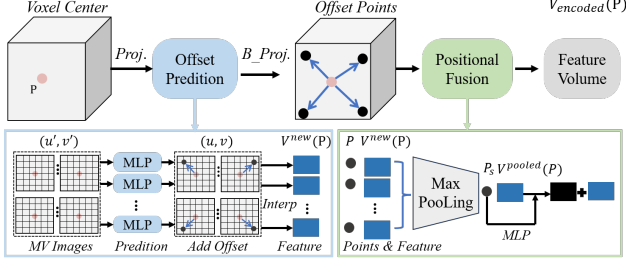


Figure 3. Illustration of **PEOM**. The voxel center is projected onto multi-view (MV) images, where each pixel coordinate predicts an offset. Features are then fused through max pooling, and the voxel position is determined based on the pixel coordinate corresponding to the maximum value. $B_Proj.$ denotes back-projection.

voxel grid has dimensions $N_x \times N_y \times N_z$, we obtain the multi-view image features corresponding to each voxel center, denoted as $V \in \mathbb{R}^{N \times N_x \times N_y \times N_z \times C}$.

3.2. Voxel optimization with PEOM

Existing related methods [31, 34, 42] rely on average pooling to generate a representation $V' \in \mathbb{R}^{N_x \times N_y \times N_z \times C}$ from V . However, that approach has two significant limitations. (i) Compromised fine detail: Due to the averaging process and voxel size, the resulting voxel representation may not accurately capture the intricate details and complex geometries of object surfaces. This can lead to the loss of critical information necessary for precise 3D object detection. (ii) Projection errors: When projecting 3D points onto the 2D image plane, inaccuracies in camera parameters can result in projection errors, further compromising the accuracy of the representation.

To address these issues, we propose the Positional Information Embedded voxel Optimization Module (PEOM), illustrated in Fig. 3. This module dynamically selects projection points and optimizes voxel positions instead of relying solely on fixed camera parameters - details below. This enhances the method’s adaptability, correcting errors caused by voxel size and camera calibration inaccuracies. The PEOM selected pixel features for the projection points more effectively represent 3D scene information.

The proposed module projects the voxel center coordinates $\mathbf{p} = (x, y, z)^\top$ onto the image plane using the available camera parameters T_i , obtaining the corresponding pixel coordinates (u'_i, v'_i) based on the projection process described in Eq. (2). The original voxel center can be located anywhere in space, disregarding foreground or background, and its image features may not contribute to object detection, potentially even hindering it. Therefore, we dynamically adjust its projection on the image. For that, we predict an offset for each pixel coordinate

$$(\Delta u_i, \Delta v_i) = \text{MLP}(F_{I_i}, \mathbf{p}), \quad (4)$$

which is applied to the pixels as

$$(u_i, v_i) = (u'_i + \Delta u_i, v'_i + \Delta v_i), \quad (5)$$

Next, we obtain the corresponding pixel features $V^{\text{new}} \in \mathbb{R}^{N \times N_x \times N_y \times N_z \times C}$ by interpolating the image feature maps at the adjusted pixel coordinates

$$V_i^{\text{new}}(\mathbf{p}) = \text{interpolate}(F_{I_i}, (u_i, v_i)), \quad (6)$$

where $V_i^{\text{new}}(\mathbf{p})$ represents the voxel feature at position \mathbf{p} from the i -th view. We acquire multi-view image features and perform max pooling to retain the most significant features. Max pooling fusion of features preserves the critical information within the voxel features, and compared to average pooling, it reduces noise impact, thereby enhancing the overall quality and stability of the 3D features.

$$V^{\text{pooled}}(\mathbf{p}) = \max_{i=1}^N V_i^{\text{new}}(\mathbf{p}), \quad (7)$$

Here, $V^{\text{pooled}} \in \mathbb{R}^{N_x \times N_y \times N_z \times C}$ represents the resulting feature map after max pooling. We select the corresponding 3D coordinates by identifying the positions with the maximum responses from the encoded features:

$$\mathbf{p}_s = \arg \max_{\mathbf{p}} V^{\text{new}}(\mathbf{p}), \quad (8)$$

This process ensures that the selected 3D coordinates accurately represent the scene’s 3D information by utilizing multi-view features and dynamic point selection. Then, the 3D positions are encoded using an Encoder module and combined with the voxel features.

$$V_{\text{encod}}(\mathbf{p}) = V^{\text{pooled}}(\mathbf{p}) + \text{Encoder}(\mathbf{p}_s), \quad (9)$$

Finally, we obtain the optimized voxel positions \mathbf{p}_s and features $V_{\text{encod}}(\mathbf{p})$.

3.3. The NeRF branch

Constructing high-quality voxel features through multi-view information is fundamental for effective 3D object detection. However, it faces the challenge of lack of geometric information that can account for occlusions [34]. Previous methods [31] have relied on dense, geometry-unaware voxels, which impede accurate object detection. NeRF-Det [42] introduces a G-MLP branch shared with a basic NeRF module to generate opacity fields that capture scene geometry. Nevertheless, their opacity estimation remains suboptimal. Our experiments verify that the contribution of the NeRF branch to the overall detection accuracy remains limited. This happens because (i) such an approach only focuses on the overall scene geometry without emphasizing the modeling of object-specific regions. To retain computational efficiency, larger voxel sizes must be chosen, and calculating the opacity of voxel center points does

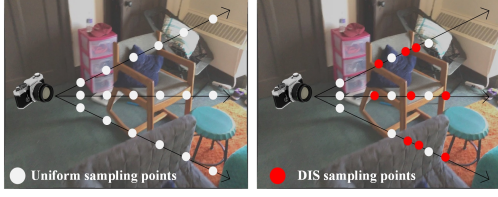


Figure 4. Illustration of **Double Important Sampling** effect. First, uniform sampling is performed, followed by CDF estimation based on the densities of the sampled points. Then, the foreground points with higher density are sampled.

not accurately represent the opacity of the entire voxel region. (ii) The voxel prediction is conducted on a point-by-point basis, leading to inconsistencies across different viewpoints. To address these issues, we propose double important sampling and Opacity Optimization Module (OOM) in our NeRF branch.

Double Important Sampling (DIS). Foreground points are widely recognised for their pivotal role in point-based 3D object detection [2, 16]. Correspondingly, in multi-view detection, we should focus more on the foreground regions and ensure the accuracy of opacity calculation for the foreground voxels. To ensure that, we propose Double Important Sampling (DIS) strategy, which considers both voxel density and pre-rendered density. The DIS ensures the accuracy of opacity predictions for foreground regions.

To implement DIS, we uniformly sample along the ray, where the initial uniform sampling depth values are calculated as follows

$$z_i = z_{\text{near}} + i \cdot \Delta z, \quad i = 0, 1, \dots, N_{\text{samples}} - 1, \quad (10)$$

$$\Delta z = \frac{z_{\text{far}} - z_{\text{near}}}{N_{\text{samples}} - 1}, \quad (11)$$

This ensures that the depth sampling is evenly distributed between z_{near} and z_{far} with N_{samples} representing the total number of samples along the ray. The sampling points are then obtained as

$$\mathbf{p}_i = \mathbf{o} + z_i \mathbf{d}, \quad (12)$$

where \mathbf{o} is the ray origin and \mathbf{d} is the view direction. We compute the density ρ_i^m at each sampling point \mathbf{p}_i using the MLP of the NeRF branch. Additionally, based on the proximity of each sampling point to the voxel grid, we compute ρ_i^v as

$$\rho_i^v = \left(\frac{1}{k} \sum_{j=1}^k \|\mathbf{p}_i - \mathbf{p}_{i_j}\| \right)^{-1}, \quad (13)$$

where \mathbf{p}_{i_j} is the position of the j -th nearest voxel center to the sampling point \mathbf{p}_i , k represents the number of nearest neighbors, and $\|\cdot\|$ denotes the Euclidean distance.

The normalized weights of each component are first

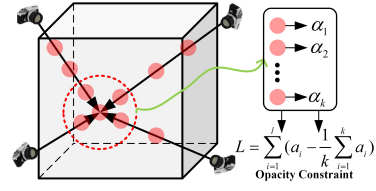


Figure 5. Illustration of loss for **Opacity Optimization Module**.

computed as follows

$$\hat{\rho}_i^m = \frac{\rho_i^m}{\left(\sum_{j=1}^{N_{\text{samples}}} \rho_j^m \right) + \epsilon}, \quad \hat{\rho}_i^v = \frac{\rho_i^v}{\left(\sum_{j=1}^{N_{\text{samples}}} \rho_j^v \right) + \epsilon}, \quad (14)$$

where ϵ is a small constant for numerical stability. The weight for each sampling point is computed as

$$w_i = \alpha \hat{\rho}_i^m + \beta \hat{\rho}_i^v, \quad (15)$$

where α and β are coefficients that balance the contributions of $\hat{\rho}_i^m$ and $\hat{\rho}_i^v$. Using the normalized weights, the Cumulative Distribution Function (CDF) is calculated as

$$\text{CDF}_i = \sum_{j=1}^i w_j, \quad (16)$$

We then generate N_{fine} uniformly distributed random variables $u_k \sim \mathcal{U}(0, 1) : k = 1, 2, \dots, N_{\text{fine}}$. New depth values are obtained through inverse sampling of the CDF as

$$z_k^{\text{fine}} = \text{CDF}^{-1}(u_k), \quad (17)$$

Finally, the new 3D points are calculated as

$$\mathbf{p}_k^{\text{fine}} = \mathbf{o} + z_k^{\text{fine}} \mathbf{d}, \quad (18)$$

These importance-sampled points are then used for further processing. Figure 4 illustrates the effect of DIS.

Opacity Optimization Module (OOM). When the same voxel is observed from multiple perspectives, it should maintain consistent opacity. This property is critical for accurate 3D reconstruction.

By enforcing opacity consistency, noise introduced by viewpoint variations can be reduced, resulting in smoother and more natural 3D voxel features.

As illustrated in Fig. 5, a point in space is observed from K different viewpoints, resulting in K predicted opacities. To ensure multi-view consistency, these opacities must be kept consistent. To that end, we propose an opacity consistency loss as follows

$$\mathcal{L}_{\text{opacity}} = \frac{1}{M} \sum_{j=1}^M \sum_{i=1}^K (\alpha_{i,j} - \bar{\alpha}_j)^2, \quad (19)$$

where $\alpha_{i,j}$ is the predicted opacity of the j -th point from the i -th viewpoint, $\bar{\alpha}_j$ is the mean opacity of the j -th point over all K viewpoints, and M is the total number of points.

ScanNet V2	mAP@0.25	cab	bed	chair	sofa	table	door	wind	bkshf	pic	cntr	desk	curt	fridge	showr	toil	sink	bath	ofurn
ImVoxelNet [31]	48.4	34.5	83.6	72.6	71.6	54.2	30.3	14.8	42.6	0.8	40.8	65.3	18.3	52.2	40.9	90.4	53.3	74.9	33.1
NeRF-Det-R50 [42]	52.0	37.2	84.8	75.0	75.6	51.4	31.8	20.0	40.3	0.1	51.4	69.1	29.2	58.1	61.4	91.5	47.8	75.1	33.6
NeRF-Det-R50* [42]	51.8	37.7	84.1	74.5	71.8	54.2	34.2	17.4	51.6	0.1	54.2	71.3	16.7	54.5	55.0	92.1	50.7	73.8	34.1
NeRF-Det-R101* [42]	53.3	37.6	84.9	76.2	76.7	57.5	36.4	17.8	47.0	2.5	49.2	52.0	29.2	68.2	49.3	97.1	57.6	83.6	35.9
ImGeoNet [34]	54.8	38.7	86.5	76.6	75.7	59.3	42.0	28.1	59.2	4.3	42.8	71.5	36.9	51.8	44.1	95.2	58.0	79.6	36.8
NeRF-Det+++ [12]	53.3	38.7	85.0	73.2	78.1	56.3	35.1	22.6	45.5	1.9	50.7	72.6	26.5	59.4	55.0	93.1	49.7	81.6	34.1
NeRF-Dets* [13]	57.5	43.7	83.8	78.3	83.0	56.8	43.2	28.8	52.0	3.8	70.5	69.8	28.5	59.4	61.6	93.1	52.4	83.3	44.5
MVSDet* [44]	56.2	40.5	82.4	79.2	80.2	55.6	40.3	25.4	60.9	3.5	47.3	73.4	28.9	64.6	64.1	94.8	52.1	76.7	41.8
GO-N3rDet-R50	56.3	40.8	86.2	79.9	80.3	55.6	36.7	30.4	60.3	4.2	52.5	70.4	41.5	53.0	53.3	94.8	55.5	78.2	39.1
GO-N3rDet-R50*	57.4	42.3	83.2	78.4	81.1	60.2	38.8	25.3	56.8	4.7	57.2	71.2	38.0	66.3	59.8	94.8	53.5	79.2	40.5
GO-N3rDet-R101*	58.6	44.7	87.6	80.8	81.5	58.2	38.8	28.8	63.4	4.0	55.4	72.0	45.2	58.9	59.0	94.8	56.5	79.5	45.3

Table 1. Results on ScanNet validation set [7] with mAP@0.25. * denotes that the model with depth rendering supervision. R50 and R101 refer to the ResNet50 and ResNet101 backbone networks, respectively.

In NeRF, opacity is computed by accumulating the densities of multiple samples along the direction of a light ray. As the distance along the ray increases, the number of samples traversed also increases, and small errors in each sample can accumulate, resulting in larger overall errors in opacity calculation. During propagation, light rays are subject to attenuation and scattering effects, which become more pronounced over longer distances. This implies that observations of distant points are relatively less reliable, and their opacity estimates are likely to have larger errors.

To mitigate these cumulative errors, we propose using distance as a weight to compute a weighted average of the densities. Specifically, by reducing the influence of distant points in the weighted average, the impact of cumulative errors on the final result can be minimized, thereby enhancing the reliability of the reconstruction. We compute the weighted average density (opacity) for the j -th point as

$$\bar{\rho}_j = \frac{\sum_{i=1}^K w_{i,j} \rho_{i,j}}{\sum_{i=1}^K w_{i,j}}, \quad (20)$$

where the weight $w_{i,j}$ for the i -th viewpoint and j -th point is inversely proportional to the distance

$$w_{i,j} = \frac{1}{d_{i,j} + \epsilon}, \quad (21)$$

and $d_{i,j}$ is the distance from the i -th viewpoint to the j -th point, ϵ allows numerical stability, and $\rho_{i,j}$ is the density (opacity) of the j -th point as observed from the i -th viewpoint. We adjust the voxel feature using optimized opacity

$$V_{\text{adjusted}}(\mathbf{p}_j) = V_{\text{encoded}}(\mathbf{p}_j) \cdot \bar{\rho}_j, \quad (22)$$

where $V_{\text{adjusted}}(\mathbf{p}_j)$ is the adjusted voxel feature at position \mathbf{p}_j , $V_{\text{encoded}}(\mathbf{p}_j)$ is the original encoded voxel feature at \mathbf{p}_j , and $\bar{\rho}_j$ is the voxel’s weighted average density (opacity).

3.4. Detection Head and Training Objective

To allow a fair evaluation of our contributions, we adopt the indoor detection head and related parameter settings as

ARKITScenes	mAP@0.25	mAP@0.5
ImVoxelNet [31]	23.6	-
NeRF-Det [42]	26.7	14.4
GO-N3rDet-R50	44.7	21.9

Table 2. Results on ARKITScenes [1] validation set.

NeRF-Det [42] and ImVoxelNet [31]. It is noteworthy that we do not use the centerness loss, as we found it less effective. We train our entire network in an end-to-end manner using a newly proposed composite loss function, defined as

$$L = L_{cls} + L_{opacity} + L_{loc} + L_c + L_d. \quad (23)$$

Here, L_{cls} and L_{loc} represent the losses for object class prediction and bounding box prediction, respectively. L_c represents the photo-metric loss. If depth maps are utilized, L_d represents the depth map rendering loss. $L_{opacity}$ denotes the opacity consistency loss, with details provided in Eq. (19).

4. Evaluation

Datasets. We follow the settings of prior methods in 3D object detection and evaluate our GO-N3rDet on two indoor object detection datasets; namely, ScanNet [7] and ARKITScenes [1]. ScanNet contains 1,513 complex indoor scenes with approximately 2.5M RGB-D frames. ARKITScenes [1] contains around 1.6K rooms with more than 5,000 scans. We primarily evaluate methods on these datasets using mAP at 0.25 IoU and 0.5 IoU threshold.

Implementation. Our approach integrates detection and NeRF-based scene representation within a unified framework. It is implemented using the MMDetection3D framework [6], optimized for 3D object detection and scene geometry perception. Further implementation details are provided in the supplementary material.

4.1. Main results

Quantitative comparison. As shown in Table 1, without relying on additional techniques, our method surpasses

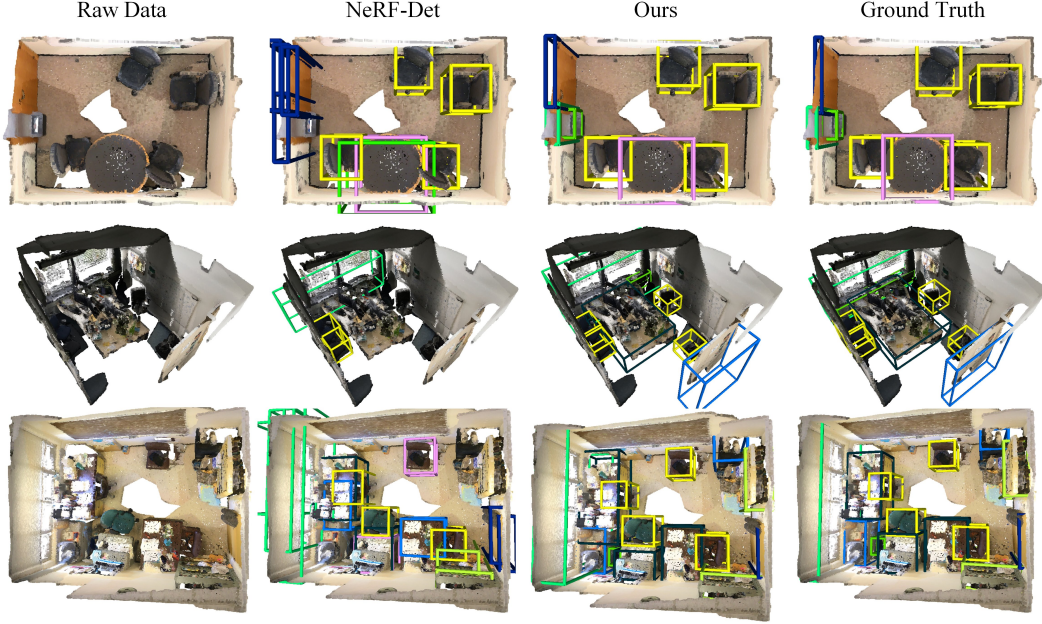


Figure 6. Representative qualitative results on ScanNet dataset [7]. As compared to the baseline, NeRF-Det [18], our GO-N3RDet not only enables precise detection of more challenging objects, but also reduces false positive detections. Best viewed on screen.

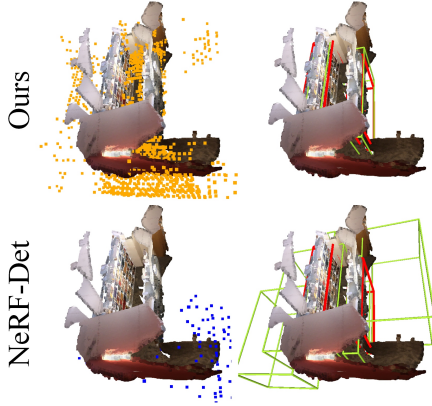


Figure 7. Impact of scene geometry awareness. Dots in left column indicate detected free-space. Our method predicts the free-space accurately, leading to less false positives and precise bounding boxes in the right column.

Method	Train epochs	Grid size	mAP@0.25
CN-RMA [33]	80+12+100	[192,192,80]	58.6
Ours	14	[40,40,16]	58.6

Table 3. Comparison of CN-RMA [33] and our method based on training epochs, grid size, and mAP@0.25.

all NeRF-based multi-view 3D detectors on the ScanNet dataset [7]. As compared to the foundational multi-view method, imVoxelNet [31], our approach achieves an absolute 10.2% improvement in the mAP@0.25 metric. Moreover, we demonstrate substantial improvements over three recent NeRF-based methods: NeRF-Det [42], NeRF-Det++ [12], and NeRF-Dets [13].

On the ARKITScenes dataset [1], we again outperform existing NeRF-based methods. As illustrated in Table 2, our approach achieves a considerable performance gain over NeRF-Det. Given the unavailability of public results for competing methods on this dataset, we locally reproduced NeRF-Det results. CN-RMA [33] is not a NeRF-based method, but it has shown strong performance in multi-view tasks by utilizing Ray Marching Aggregation to capture detailed scene geometry. Given its effectiveness in these scenarios, we compared our method with CN-RMA to evaluate performance and efficiency. As the Table 3 shows, our approach achieves the same mAP@0.25 of 58.6 as CN-RMA, but with $\sim 14\times$ fewer training epochs. Additionally, our method uses a much smaller grid size, demonstrating that we achieve comparable accuracy with far less computational complexity and training time. Unlike CN-RMA, which requires ground truth TSDF [33] supervision, our method achieves comparable performance without it, reducing reliance on costly ground truth geometry.

Qualitative comparison. We compare the predicted 3D bounding boxes generated by GO-N3RDet against NeRF-Det [42] to demonstrate the superior geometric scene perception of our approach. As shown in Fig. 6, GO-N3RDet consistently performs better in both simple and complex environments. In the complex environment of the second row, NeRF-Det [42] missed several key objects, including the desk, cabinet, garbage bin, and door. In contrast, GO-N3RDet successfully detected all relevant objects. In the highly challenging scene shown in the third row, NeRF-Det [42] exhibits multiple false positives and missed detec-

tions, while GO-N3RDet closely matches the ground truth. Its predicted bounding boxes are compact and accurate. We refer to the supplementary material for more examples.

Impact of scene geometry perception. As shown in Fig. 7, we compare the scene geometry perception capabilities of NeRF-Det [42] and our GO-N3RDet. In the left column, the points represent free space (low-opacity areas) predicted by each method. The right column presents the ground truth (red boxes) alongside the predicted bounding boxes results (green) from both methods. NeRF-Det [42] detects free space inaccurately, leading to false positives. In contrast, our method provides a more accurate understanding of the scene’s geometry, predicting better opacity levels and, consequently, delivering more precise object detection.

4.2. Ablation Study and Discussion

Effect of sub-modules. We conduct an extensive ablation study to analyze the contribution of different sub-modules to our method. Table 4 reports mAP@0.25 results on the ScanNet dataset [7]. The Naive approach refers to constructing voxel features using the method described in § 3.1, followed by directly employing a voxel-based detection head for the detection experiments. It can be observed that when PEOM (§ 3.1), DIS (§ 3.3), and OOM (§ 3.3) are applied, each contributes to a notable improvement in the detection performance, demonstrating the effectiveness of each module. Best results are achieved by combining them.

The effect of opacity. We also validate the effect of opacity adjustment across different methods. Opacity adjustment is crucial for perceiving scene geometry. Table 5 provides a quantitative analysis of the effect of opacity. We conducted detection experiments with NeRF-Det [42] and our GO-N3rRDet, both with and without opacity-adjusted voxel features. It can be observed that in NeRF-Det, the presence or absence of opacity adjustment does not significantly affect the final results. In NeRF-Det, we removed the opacity prediction branch, and despite not utilizing opacity to adjust voxel features, the precision at mAP@0.25 only decreased by 0.2%. This suggests that opacity did not significantly enhance the model’s ability to perceive geometric information. In contrast, in our GO-N3RDet, opacity modulation led to 3.4% and 4.3% improvement in precision.

Number of sampling points. We also conducted a comprehensive study to evaluate the effect of different sampling strategies on detection performance. As shown in Tab. 6, increasing the number of sampling points with Uniform Sampling (Us), as employed in NeRF-Det [42], resulted in minimal improvements. However, even when keeping the number of sampling points fixed at 64 per ray while employing DIS, our method achieves a score of 54.2, surpassing the 53.2 achieved by uniform sampling. Furthermore, with DIS, using 128 sampling points leads to a notable performance boost, highlighting the superior efficacy of our DIS

Naive	✓	✓	✓	✓	✓
POEM		✓			✓
DIS			✓		✓
OOM				✓	✓
mAP@0.25	48.4	55.2	55.3	53.8	58.6

Table 4. Contribution of sub-modules (ScanNet dataset).

Method	NeRF-Det		Ours	
	mAP@0.25	mAP@0.5	mAP@0.25	mAP@0.5
W/O	53.1	26.9	55.2	29.4
W	53.3(+0.2)	27.4(+0.5)	58.6(+3.4)	33.7(+4.3)

Table 5. Impact of opacity adjustment. “W” refers to voxel features with opacity adjustment, while “W/O ” refers to without.

Method	mAp@0.25	mAp@0.5
Us 64	53.2	27.6
Us 128	53.0	27.2
DIS 64	54.2	28.2
Us 64 + DIS 64	54.7	27.8
DIS 128	55.3	29.2

Table 6. Comparison of sampling methods using ScanNet dataset. “Us” denotes Uniform sampling. The number of samples used are mentioned in each row. DIS 128 gives the best results.

module in enhancing detection precision.

5. Conclusion

In this paper, we presented GO-N3RDet, an end-to-end network architecture that leverages NeRF and enhance geometric perception of multi-view voxel scenes, thereby improving the state-of-the-art for 3D object detection. The constituent PEOM module of our metho integrates multi-view features and enriches voxel representations with precise 3D positional information. To enhance opacity prediction accuracy, a DIS module focuses on foreground regions by considering the density from both NeRF predictions and voxel grid inferences, while our OOM module ensures accurate opacity calculation and consistency across multiple views. Qualitative and quantitative results demonstrate the effectiveness of GO-N3RDet in accurately reconstructing scene geometry and improving detection reliability.

Acknowledgement. This work was supported by NSFC (62373140, U21A20487, U2013203), Leading Talents in Science and Technology Innovation of Hunan Province (2023RC1040), the Project of Science Fund of Hunan Province (2022JJ30024); the Project of Talent Innovation and Sharing Alliance of Quanzhou City (2021C062L). This work was completed by Zechuan Li during his visit to the University of Melbourne under the supervision of Naveed Akhtar and Hongshan yu. Zechuan Li, Hongshan Yu are with the School of Robotics, College of Electrical and Information Engineering, Quanzhou Institute of Industrial Design and Machine Intelligence Innovation, Hunan University.

References

- [1] Gilad Baruch, Zhuoyuan Chen, Afshin Dehghan, Tal Dimry, Yuri Feigin, Peter Fu, Thomas Gebauer, Brandon Joffe, Daniel Kurz, Arik Schwartz, et al. Arkitscenes: A diverse real-world dataset for 3d indoor scene understanding using mobile rgb-d data. *arXiv preprint arXiv:2111.08897*, 2021. 2, 6, 7
- [2] Chen Chen, Zhe Chen, Jing Zhang, and Dacheng Tao. Sasa: Semantics-augmented set abstraction for point-based 3d object detection. In *Proceedings of the AAAI Conference on Artificial Intelligence*, volume 36, pages 221–229, 2022. 5
- [3] Xiaozhi Chen, Kaustav Kundu, Yukun Zhu, Andrew G Berneshawi, Huimin Ma, Sanja Fidler, and Raquel Urtasun. 3d object proposals for accurate object class detection. *Advances in neural information processing systems*, 28, 2015. 3
- [4] Xiaozhi Chen, Huimin Ma, Ji Wan, Bo Li, and Tian Xia. Multi-view 3d object detection network for autonomous driving. In *Proceedings of the IEEE conference on Computer Vision and Pattern Recognition*, pages 1907–1915, 2017. 3
- [5] Bowen Cheng, Lu Sheng, Shaoshuai Shi, Ming Yang, and Dong Xu. Back-tracing representative points for voting-based 3d object detection in point clouds. In *Proceedings of the IEEE/CVF Conference on Computer Vision and Pattern Recognition*, pages 8963–8972, 2021. 2
- [6] MMDetection3D Contributors. MMDetection3D: OpenMMLab next-generation platform for general 3D object detection. <https://github.com/open-mmlab/mmdetection3d>, 2020. 6
- [7] Angela Dai, Angel X Chang, Manolis Savva, Maciej Halber, Thomas Funkhouser, and Matthias Nießner. Scannet: Richly-annotated 3d reconstructions of indoor scenes. In *Proceedings of the IEEE conference on computer vision and pattern recognition*, pages 5828–5839, 2017. 2, 6, 7, 8
- [8] JunYoung Gwak, Christopher Choy, and Silvio Savarese. Generative sparse detection networks for 3d single-shot object detection. In *Computer Vision—ECCV 2020: 16th European Conference, Glasgow, UK, August 23–28, 2020, Proceedings, Part IV 16*, pages 297–313. Springer, 2020. 2, 3
- [9] Kaiming He, Georgia Gkioxari, Piotr Dollár, and Ross Girshick. Mask r-cnn. In *Proceedings of the IEEE international conference on computer vision*, pages 2961–2969, 2017. 1
- [10] Kaiming He, Xiangyu Zhang, Shaoqing Ren, and Jian Sun. Deep residual learning for image recognition. In *Proceedings of the IEEE conference on computer vision and pattern recognition*, pages 770–778, 2016. 3
- [11] Benran Hu, Junkai Huang, Yichen Liu, Yu-Wing Tai, and Chi-Keung Tang. Nerf-rpn: A general framework for object detection in nerfs. In *IEEE/CVF Conference on Computer Vision and Pattern Recognition (CVPR)*, 2023. 1, 3
- [12] Chenxi Huang, Yuenan Hou, Weicai Ye, Di Huang, Xiaoshui Huang, Binbin Lin, Deng Cai, and Wanli Ouyang. Nerf-det++: Incorporating semantic cues and perspective-aware depth supervision for indoor multi-view 3d detection. *arXiv preprint arXiv:2402.14464*, 2024. 1, 3, 6, 7
- [13] Chi Huang, Xinyang Li, Shengchuan Zhang, Liujuan Cao, and Rongrong Ji. Nerf-dets: Enhancing multi-view 3d object detection with sampling-adaptive network of continuous nerf-based representation. *arXiv preprint arXiv:2404.13921*, 2024. 1, 3, 6, 7
- [14] Siyuan Huang, Yixin Chen, Tao Yuan, Siyuan Qi, Yixin Zhu, and Song-Chun Zhu. Perspectivenet: 3d object detection from a single rgb image via perspective points. *Advances in neural information processing systems*, 32, 2019. 1
- [15] Siyuan Huang, Siyuan Qi, Yinxue Xiao, Yixin Zhu, Ying Nian Wu, and Song-Chun Zhu. Cooperative holistic scene understanding: Unifying 3d object, layout, and camera pose estimation. *Advances in Neural Information Processing Systems*, 31, 2018. 3
- [16] Zechuan Li, Hongshan Yu, Zhengeng Yang, Tongjia Chen, and Naveed Akhtar. Ashapeformer: Semantics-guided object-level active shape encoding for 3d object detection via transformers. In *Proceedings of the IEEE/CVF Conference on Computer Vision and Pattern Recognition*, pages 1012–1021, 2023. 1, 2, 5
- [17] Tsung-Yi Lin, Piotr Dollár, Ross Girshick, Kaiming He, Bharath Hariharan, and Serge Belongie. Feature pyramid networks for object detection. In *Proceedings of the IEEE conference on computer vision and pattern recognition*, pages 2117–2125, 2017. 1
- [18] Zechen Liu, Zizhang Wu, and Roland Tóth. Smoke: Single-stage monocular 3d object detection via keypoint estimation. In *Proceedings of the IEEE/CVF conference on computer vision and pattern recognition workshops*, pages 996–997, 2020. 3, 7
- [19] Mikołaj Łysakowski, Kamil Żywanowski, Adam Banaszczyk, Michał R Nowicki, Piotr Skrzypczyński, and Sławomir K Tadeja. Real-time onboard object detection for augmented reality: Enhancing head-mounted display with yolov8. In *2023 IEEE International Conference on Edge Computing and Communications (EDGE)*, pages 364–371. IEEE, 2023. 1
- [20] Ben Mildenhall, Pratul P Srinivasan, Matthew Tancik, Jonathan T Barron, Ravi Ramamoorthi, and Ren Ng. Nerf: Representing scenes as neural radiance fields for view synthesis. *Communications of the ACM*, 65(1):99–106, 2021. 1, 2
- [21] Ali Mohammadkhorsani, Kaveh Malek, Rushil Mojidra, Jian Li, Caroline Bennett, William Collins, and Fernando Moreu. Augmented reality-computer vision combination for automatic fatigue crack detection and localization. *Computers in Industry*, 149:103936, 2023. 1
- [22] Yinyu Nie, Xiaoguang Han, Shihui Guo, Yujian Zheng, Jian Chang, and Jian Jun Zhang. Total3dunderstanding: Joint layout, object pose and mesh reconstruction for indoor scenes from a single image. In *Proceedings of the IEEE/CVF Conference on Computer Vision and Pattern Recognition*, pages 55–64, 2020. 1
- [23] Songyou Peng, Kyle Genova, Chiyu “Max” Jiang, Andrea Tagliasacchi, Marc Pollefeys, and Thomas Funkhouser. Openscene: 3d scene understanding with open vocabularies. In *Proceedings of the IEEE/CVF Conference on Computer Vision and Pattern Recognition (CVPR)*, pages 815–824, June 2023. 1

- [24] Charles R Qi, Xinlei Chen, Or Litany, and Leonidas J Guibas. Imvotenet: Boosting 3d object detection in point clouds with image votes. In *Proceedings of the IEEE/CVF conference on computer vision and pattern recognition*, pages 4404–4413, 2020. 1
- [25] Charles R Qi, Or Litany, Kaiming He, and Leonidas J Guibas. Deep hough voting for 3d object detection in point clouds. In *proceedings of the IEEE/CVF International Conference on Computer Vision*, pages 9277–9286, 2019. 1
- [26] Charles R Qi, Or Litany, Kaiming He, and Leonidas J Guibas. Deep hough voting for 3d object detection in point clouds. In *proceedings of the IEEE/CVF International Conference on Computer Vision*, pages 9277–9286, 2019. 2
- [27] Charles R Qi, Hao Su, Kaichun Mo, and Leonidas J Guibas. Pointnet: Deep learning on point sets for 3d classification and segmentation. In *Proceedings of the IEEE conference on computer vision and pattern recognition*, pages 652–660, 2017. 2
- [28] Charles Ruizhongtai Qi, Li Yi, Hao Su, and Leonidas J Guibas. Pointnet++: Deep hierarchical feature learning on point sets in a metric space. *Advances in neural information processing systems*, 30, 2017. 2
- [29] Joseph Redmon, Santosh Divvala, Ross Girshick, and Ali Farhadi. You only look once: Unified, real-time object detection. In *Proceedings of the IEEE conference on computer vision and pattern recognition*, pages 779–788, 2016. 1
- [30] Anna Rukhovich, Danila anFd Vorontsova, and Anton Konushin. Fcaf3d: Fully convolutional anchor-free 3d object detection. In *European Conference on Computer Vision*. Springer, 2022. 2
- [31] Danila Rukhovich, Anna Vorontsova, and Anton Konushin. Imvoxelnet: Image to voxels projection for monocular and multi-view general-purpose 3d object detection. In *Proceedings of the IEEE/CVF Winter Conference on Applications of Computer Vision*, pages 2397–2406, 2022. 1, 3, 4, 6, 7
- [32] Danila Rukhovich, Anna Vorontsova, and Anton Konushin. Tr3d: Towards real-time indoor 3d object detection. *arXiv preprint arXiv:2302.02858*, 2023. 3
- [33] Guanlin Shen, Jingwei Huang, Zhihua Hu, and Bin Wang. Cn-rma: Combined network with ray marching aggregation for 3d indoor object detection from multi-view images. In *Proceedings of the IEEE/CVF Conference on Computer Vision and Pattern Recognition (CVPR)*, pages 21326–21335, June 2024. 2, 3, 7
- [34] Tao Tu, Shun-Po Chuang, Yu-Lun Liu, Cheng Sun, Ke Zhang, Donna Roy, Cheng-Hao Kuo, and Min Sun. Imgeonet: Image-induced geometry-aware voxel representation for multi-view 3d object detection. In *Proceedings of the IEEE/CVF International Conference on Computer Vision*, pages 6996–7007, 2023. 1, 3, 4, 6
- [35] Jingwen Wang, Hongshan Yu, Xuefei Lin, Zechuan Li, Wei Sun, and Naveed Akhtar. Efrnet-vl: An end-to-end feature refinement network for monocular visual localization in dynamic environments. *Expert Systems with Applications*, 243:122755, 2024. 1
- [36] Tai Wang, ZHU Xinge, Jiangmiao Pang, and Dahua Lin. Probabilistic and geometric depth: Detecting objects in perspective. In *Conference on Robot Learning*, pages 1475–1485. PMLR, 2022. 3
- [37] Tai Wang, Xinge Zhu, Jiangmiao Pang, and Dahua Lin. Fcos3d: Fully convolutional one-stage monocular 3d object detection. In *Proceedings of the IEEE/CVF International Conference on Computer Vision*, pages 913–922, 2021. 3
- [38] Yan Wang, Wei-Lun Chao, Divyansh Garg, Bharath Hariharan, Mark Campbell, and Kilian Q Weinberger. Pseudolidar from visual depth estimation: Bridging the gap in 3d object detection for autonomous driving. In *Proceedings of the IEEE/CVF conference on computer vision and pattern recognition*, pages 8445–8453, 2019. 3
- [39] Qian Xie, Yu-Kun Lai, Jing Wu, Zhoutao Wang, Dening Lu, Mingqiang Wei, and Jun Wang. Venet: Voting enhancement network for 3d object detection. In *Proceedings of the IEEE/CVF International Conference on Computer Vision*, pages 3712–3721, 2021. 2
- [40] Qian Xie, Yu-Kun Lai, Jing Wu, Zhoutao Wang, Yiming Zhang, Kai Xu, and Jun Wang. Mlcvnet: Multi-level context votenet for 3d object detection. In *Proceedings of the IEEE/CVF conference on computer vision and pattern recognition*, pages 10447–10456, 2020. 2
- [41] Yiming Xie, Huaizu Jiang, Georgia Gkioxari, and Julian Straub. Pixel-aligned recurrent queries for multi-view 3D object detection. In *ICCV*, 2023. 3
- [42] Chenfeng Xu, Bichen Wu, Ji Hou, Sam Tsai, Ruilong Li, Jialiang Wang, Wei Zhan, Zijian He, Peter Vajda, Kurt Keutzer, et al. Nerf-det: Learning geometry-aware volumetric representation for multi-view 3d object detection. In *Proceedings of the IEEE/CVF International Conference on Computer Vision*, pages 23320–23330, 2023. 1, 3, 4, 6, 7, 8
- [43] Danfei Xu, Dragomir Anguelov, and Ashesh Jain. Pointfusion: Deep sensor fusion for 3d bounding box estimation. In *Proceedings of the IEEE conference on computer vision and pattern recognition*, pages 244–253, 2018. 3
- [44] Yating Xu, Chen Li, and Gim Hee Lee. Mvsdet: Multi-view indoor 3d object detection via efficient plane sweeps. In *Proceedings of the 38th Conference on Neural Information Processing Systems (NeurIPS)*, 2024. 3, 6
- [45] Yan Yan, Yuxing Mao, and Bo Li. Second: Sparsely embedded convolutional detection. *Sensors*, 18(10):3337, 2018. 2
- [46] Cheng Zhang, Zhaopeng Cui, Yinda Zhang, Bing Zeng, Marc Pollefeys, and Shuaicheng Liu. Holistic 3d scene understanding from a single image with implicit representation. In *Proceedings of the IEEE/CVF Conference on Computer Vision and Pattern Recognition*, pages 8833–8842, 2021. 1
- [47] Cheng Zhang, Zhaopeng Cui, Yinda Zhang, Bing Zeng, Marc Pollefeys, and Shuaicheng Liu. Holistic 3d scene understanding from a single image with implicit representation. In *Proceedings of the IEEE/CVF Conference on Computer Vision and Pattern Recognition*, pages 8833–8842, 2021. 3
- [48] Zaiwei Zhang, Bo Sun, Haitao Yang, and Qixing Huang. H3dnet: 3d object detection using hybrid geometric primitives. In *European Conference on Computer Vision*, pages 311–329. Springer, 2020. 2
- [49] Hongyu Zhou, Jiahao Shao, Lu Xu, Dongfeng Bai, Weichao Qiu, Bingbing Liu, Yue Wang, Andreas Geiger, and Yi

- Liao. Hugs: Holistic urban 3d scene understanding via gaussian splatting. In *Proceedings of the IEEE/CVF Conference on Computer Vision and Pattern Recognition (CVPR)*, pages 21336–21345, June 2024. [1](#)
- [50] Yanmei Zou, Hongshan Yu, Zhengeng Yang, Zechuan Li, and Naveed Akhtar. Improved mlp point cloud processing with high-dimensional positional encoding. In *Proceedings of the AAAI Conference on Artificial Intelligence*, volume 38, pages 7891–7899, 2024. [1](#)
- [51] Zhengxia Zou, Keyan Chen, Zhenwei Shi, Yuhong Guo, and Jieping Ye. Object detection in 20 years: A survey. *Proceedings of the IEEE*, 111(3):257–276, 2023. [1](#)